# Preliminary P-Stacks

by Philip S. Schultz

In this section we show an example of slant stacks applied to field data (supplied to us by Western Geophysical Inc.).

The simple slant stack with no velocity mute (see Claerbout SEP-5, p. 1) was applied to the data in both common geophone gathers and common shot gathers. Three numerical values of the ray parameter, $p$, were chosen for the stack ( $p = 0.00007, 0.00005, 0.00003$, giving $\theta = 20.5°, 14.5°$ and $8.6°$ for water velocity). Recall that

$$p = \frac{\sin\theta}{v} = \frac{dt}{dx} \qquad (1)$$

where $\theta$ is the propagation angle from the vertical, $v$ is the velocity and $(x,t)$ are the horizontal and vertical coordinates of the common geophone or common shot gather.

Since we stacked over both common $g$ and common $s$, we obtained six slant sections from the three $p$ values. Our convention is to refer to the stacks over a common geophone with positive $p$ values, and to the stacks over common shot with negative $p$ values.

The sections were transformed to interpretation coordinates before plotting was done. The sheared look of the sections (Figures 3-8) is due to the transformation. Since a detailed derivation of interpretation coordinates is given by Claerbout("Slant Plane Wave Interpretation Coordinates", this report, page 89 ), we shall say only that these coordinates force slant stacks to resemble vertical stacks, and as a result, sections from various stacking angles can be overlain. The transformation involves both a shearing action and an NMO correction, given by equations (10a) and (10b) by Claerbout on page 93 .

We used a constant velocity in the transformation equal to

5000 fps so that we could see the effect of an incorrect transformation velocity on the deeper events.

The final seven Figures (9-15) show contiguous sets of "p-gathers" from seven different parts of the section. Traces were collected from each of the six p-sections corresponding to a common sea floor reflection point (also sub-sea floor reflection points if the earth had a constant 5000 fps velocity) and arranged in sets of mini-gathers with a format shown in Figure 1.

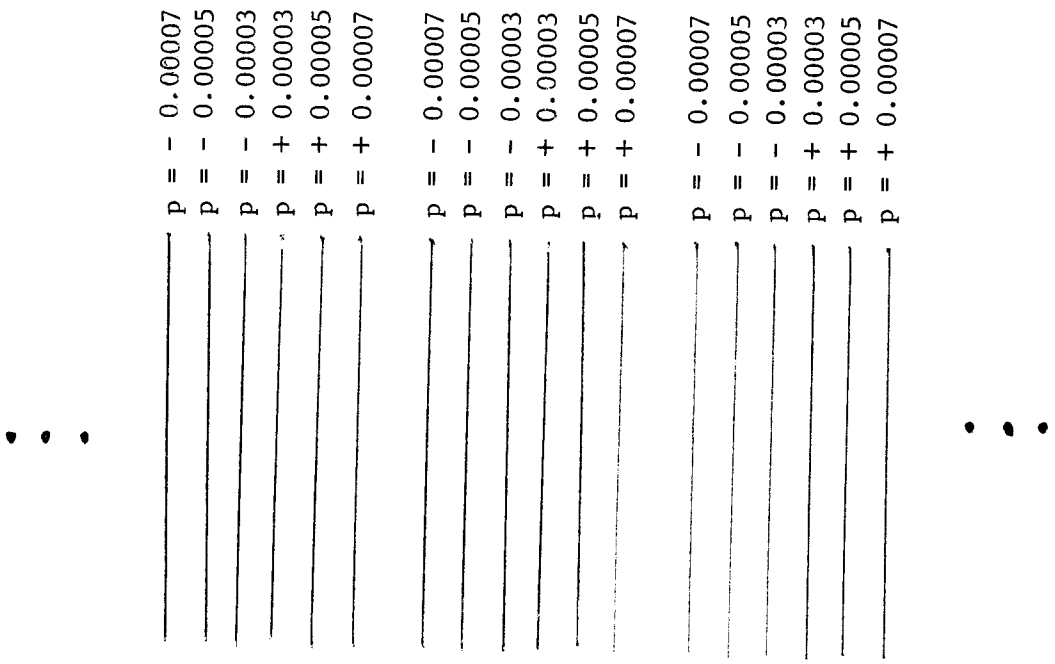


Figure 1. The format for the p-gathers of Figures 9-15.

The seven locations in the section where the p-gathers were displayed are noted in the upper margin of the p-sections.

Our interpretations of this data display are at this early stage somewhat speculative.

Figure 2.

The CDP section supplied by Western Geophysical Inc. This section is left-right reversed from the subsequent sections. Note that strong evidence of sea floor multiples remain even though CDP stacking was done to enhance the primaries. Six seconds of data are shown in all sections.

The data are 46-fold coverage taken with 46 trace streamer cable.

105

Fig. 2

Figure 3.

Slant section for $p = -0.00007$ (common shot gathers). The strongly sheared appearance is due to the transformation to interpretation coordinates. Since these stacks were done over common shot gathers, the effect of dead shots is quite apparent. All "holes" in the data are due to dead shots except for the region labeled "programming error." The clean truncation of the data at the ends of the section is due to the fact that all the common shot gathers were complete.

The propagation angle of the downgoing wave in water is noted in the upper left-hand region of the section on a one to one scale (the seismic data is not one to one).

The half-rectangles in the upper portion of this and subsequent sections show the regions from where the p-gathers were collected.

Figure 4.

Slant section for $p = -0.00005$ . The buried slope is becoming a weaker reflection. The shallow water sea floor arrival shows a characteristic waveform consistent within the section, but quite different than that of the same region in Figure 3. This phenomenon demonstrates one of the advantages of the slant frame for multiple reflection suppression: the angle-dependent antenna response and reflection coefficient remain constant within a p-section and change only from one p-section to another.

The left-hand region of the section shows one-sided diffractions sloping downward to the right from the far left data truncation and the region labeled "programming error." These can hopefully be eliminated by migration.

Figure 5.

Slant section for $p = -0.00003$ . The buried slope is now a very weak reflector. This may be due to reflection coefficient manifesting itself as a function of angle.

The sea floor primary reflection in the flat region has now a quite obviously different waveform than that in the previous two sections.

Figure 6.

Slant section for $p = + 0.00003$ (common geophone gathers). The propagation angle has now changed signs.

The truncation at the left-hand side of the section has now changed character. This is due to a 96 gather transient before a complete common geophone gather can be constructed. The gathers which created the traces to the far left were abundant in large offset traces, but deficient in near offset traces.

One-sided diffractions are also noticeable from the "programming error" region and the regions of missing (dead) shots this time sloping to the left.

The buried slope is now a very strong reflector, again probably due to angle dependent reflection coefficient.

Figure 7.

Slant section for $p = + 0.00005$ . A wing-like feature is now apparent on the non-buried region of the slope. A glance at the negative p-section shows that this area was previously very clearly delineated. This phenomenon may be due to scattering off the slope enhanced by the grazing angle of the ray (but we really haven't figured it out yet).

Figure 8.

Slant section for $p = + 0.00007$ . The wing-like feature on the non-buried region of the slope is now enhanced. The buried slope continues to be a strong reflector.

Figure 9.

P-gathers for region 1 (see Figure 1 and the top margin of Figures 3-8). The one second lines can be seen as light lines across the page. Almost four seconds of data are shown.

The sea floor primary was over-corrected for NMO, producing a "frown." The strong primary reflections between 2 and 2.3 seconds show a tendency to "smile", implying that this may be the manifestation of a positive residual velocity.

The first sea floor multiple at 2.9 seconds shows a stronger "frown" than the primary.

The buried slope at about 2.7 seconds is an example of a dipping event but is difficult to pick in this region.

Figure 10.

P-gathers for region 2. Beginning at one second is the wing-like event above the slope in the positive p-sections.

At 0.2 seconds can be seen the remnant of the direct arrival. Although the slant stack will not enhance the direct arrival, a strong signal on the inner traces will overcome the phase averaging and produce a remnant event.

Figure 11.

P-gathers for region 3. The direct arrival on the slope shows a pronounced v-character, the shorter side of the v is in the downslope direction.

Figure 12. P-gathers for region 4.

The v-character is still apparent for the sloping sea floor.

Figure 13.

P-gathers for region 5.

Figure 14.

P-gathers for region 6.

The sea floor primary begins with a "smile" character, but the multiples quickly become flat events.

Figure 15.

P-gathers for region 7.

The gentle slope is now downward to the right. The sea floor primary remains smiling while the multiples frown.

## Introduction to Engquist's Work

In SEP-2, page 296, we got a glimpse of the magnitude of the advantage of fourth order accuracy compared to second order accuracy in migration. In terms of spatial $x$ differences, a 1.5 percent accuracy occurs at 10 points per wavelength for second order and 4 points per wavelength for fourth order. There is obviously a considerable saving in computer memory in going to fourth order. Also in SEP-2, page 109 is a program which indicates a further saving in computer time when the calculation becomes explicit for a particular choice of $\Delta Z$ .

The problem of accuracy is even more acute with time differencing and time derivatives. Again in SEP-2, page 296, we see that 16 points per wavelength are required to achieve one percent accuracy on the time axis. To be honest, we have usually been doing our migrations on 4 millisec data which often corresponds to about 10 points per wavelength or about 3% accuracy. Engquist's work shows how we can use fourth order accuracy on the time derivative and also achieve fourth order accuracy on the lateral $x$ axis without restricting our choice of $\Delta z$ .

While we have not yet had time to fully analyze the implications and best use of Bjorn's results, it seems that we may reasonably hope to be able to migrate 8 millisec data with equal or slightly better accuracy than we now get on 4 millisec data. Also, the calculation should require about half the memory and roughly half the computation time. These will be important savings as migration is later applied to multiple elimination and velocity analysis.

J.F.C.